Ka-Band Diplexer for 5G mmWave Applications in Inverted Microstrip Gap Waveguide Technology

Carlos Sanchez-Cabello [1], **Luis Fernando Herran [2]** and **Eva Rajo-Iglesias [1,*]**

[1] Department of Signal Theory and Communications, University Carlos III of Madrid, 28911 Leganés, Spain; carlos.sanchez@uc3m.es

[2] Department of Signal Theory and Communications, University of Oviedo, 33003 Oviedo, Spain; herranluis@uniovi.es

[*] Correspondence: eva.rajo@uc3m.es; Tel.: +34-916-248-774

Abstract: A new cost-efficient, low-loss Ka-band diplexer designed in inverted microstrip gap waveguide technology is presented in this paper. Gap waveguide allows to propagate quasi-TEM modes in the air between two metal plates without the need for contact between them by using periodic metasurfaces. The diplexer is realized by using a bed of nails as AMC (Artificial Magnetic Conductor), first modeled with a PMC (Perfect Magnetic Conductor) surface for design simplification, and two fifth order end-coupled passband filters (BPFs) along with a power divider. The experimental verification confirms that the two channels centered at 24 GHz and 28 GHz with 1 GHz of bandwidth show measured insertion losses of 1.5 dB and 2 dB and 60 dB of isolation between them. A slight shift in frequency is observed in the measurements that can be easily explained by the variation in the permittivity of the substrate.

Keywords: gap waveguide; inverted microstrip gap; metamaterial; diplexer; mm-Wave; 5G; filter

1. Introduction

The new 5G mobile communication standard is defined to meet the increasingly pressing needs for bandwidth due to high data consumption and an increasingly lower latency in the network. This is obtained by moving much of the intelligence and algorithms necessary to the base stations themselves, moving them away from the core network. To accomplish the latter, installing networks with computing power equipment in these stations is needed, whereas to meet the other requirements of higher bandwidth is necessary to improve signal coding techniques or increase the frequency towards mm-Wave carriers. It is in the latter context where the current technology has several weaknesses, and to address them, the "gap waveguide" technology is being developed since its invention in 2009 [1]. In this technology, it is possible to propagate a quasi-TEM mode in the "Ridge" and "Inverted Microstrip" versions (a TE/TM in the "Groove" one) between parallel metal plates while periodic structures used as PMC prevent all other modes to propagate outside the propagation area [1–4].

This technology allows to transmit high-frequency signals with low loss with a moderate cost, since generally dispenses dielectrics and uses air as the medium for propagation. In addition, this technology does not require electrical contact between the top and bottom parts existing in all its versions. There are many examples of designs of antennas and circuits made in gap waveguide technology in the literature, but not that many in the case of the inverted microstrip version. Some examples can be found in [5–11]; also transitions to standard waveguides and transmission lines have been developped [12–16], the study of the optimal numeric port [17]; up to some of the various components that make up a RF front-end like antenna feeds [18–32]; beamforming Butler matrix [33,34]

or filters [5,35–39]. Few studies on diplexers with this technology have been published apart from this one using the groove version [40]. This version, like the ridge version, has less losses than the inverted microstrip because they do not use dielectrics, but at the cost of added manufacturing complexity and cost.

The purpose of this work is therefore to design a diplexer using inverted gap waveguide technology operating in Ka band. The design of the diplexer is presented in Section 2 including the analysis of losses. Section 3 contains the experimental results and finally the main conclusions are summarized in Section 4.

2. Diplexer Design

The first step of the design is the selection of the metasurface made of periodic pins and to select the type of filter to be used. The most common type of bandpass filter used in this technology is the parallel-coupled line one as in [5]. However, although for lower frequency, their operation is suitable [23], some initial studies have shown that these filters in the Ka band suffer from tolerance problems. Specifically, the sensitivity of the filter to the position of the lines w.r.t. the pins can be a problem.

These tolerances were carefully studied in [11], where the sensitivity of the inverted microstrip gap waveguide line impedance to its position on the rows of pins is studied in depth. For that reason we decided to follow the work presented in [36] where an End-Coupled Band Pass Filter (BPF) was selected. In this topology, the dependence of the coupling between lines with respect to the relative position of the lines with respect to the metasurface made with a bed of nails is much less.

2.1. Selection of the Bed of Nails

As in most of the designs made in gap waveguide technology, the selected structure to emulate the ideal PMC is a bed of nails (pins). The dimensions have been selected to provide a stop-band covering both central frequencies of the bandpass filters (24 GHz and 28 GHz). Initially the design was made using the substrate RO4003C$^{\text{TM}}$. Specifically, the dimensions of the bed of nails chosen are: *thickness* = 0.508 mm; *height* = 3 mm; *gap* = 0.5 mm, *period* = 2 mm and *side* = 1 mm. With these dimensions, a stopband going from 18.10 GHz to 29.66 GHz is obtained for RO4003C$^{\text{TM}}$ substrate as shown in Figure 1.
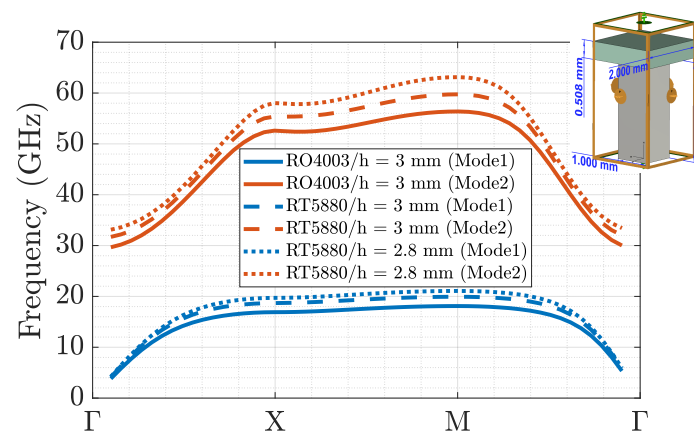

Figure 1. Dispersion diagram comparison between Rogers RT5880$^{\text{TM}}$ and RO4003C$^{\text{TM}}$ substrates (t = 0.508 mm; h = 2.8 mm or 3 mm; g = 0.5 mm, p = 2 mm, a = 1 mm).

2.2. Filters Design

First, the theoretical design of both filters using the ideal PMC boundary condition was made. Later on, the PMC was replaced by the designed bed of pins. For the design of a filter with these

characteristics, the design procedure that appears in [41] has been followed. Additionally, as in [36], the discontinuity in the microstrip line was first modeled including the effect of the pins under it, as a π-network of capacitors as it is shown in Figure 2a,b. The Y-parameters of the two-port network were calculated for different microstrip gap sizes, and then, the capacitance values were obtained with Equation (1).

$$C_g = -\frac{Im(Y_{21})}{\omega_0}; \; C_p = -\frac{Im(Y_{11} + Y_{21})}{\omega_0} \tag{1}$$

This theoretical design offers a good starting point to make the necessary adjustments using the CST Microwave Studio full wave simulator. We have selected Rogers RO4003C^{TM} as dielectric material (ε_r = 3.55 and tanδ = 0.0027 @10 GHz). Two fifth order Chebyshev end-coupled BPF were designed with a fractional bandwidth (FBW) of a 3.3% and 0.1 dB passband ripple following a classical design methodology. The center frequencies were selected as 24 GHz and 28 GHz, respectively.

An example of the filter design is shown in Figure 3. In this figure the performance of the PMC starting case is compared with the real design made with pins; and, for the latter case, both ideal lossless and the lossy cases are represented. Insertion losses of 1.6 dB are observed. The agreement of the PMC case and the ideal pins is very good.
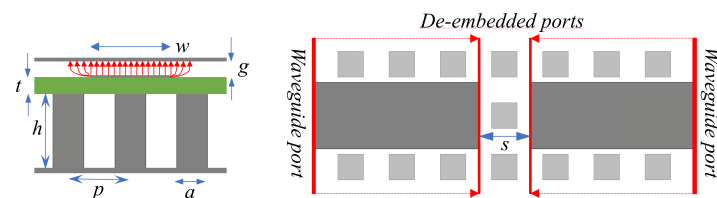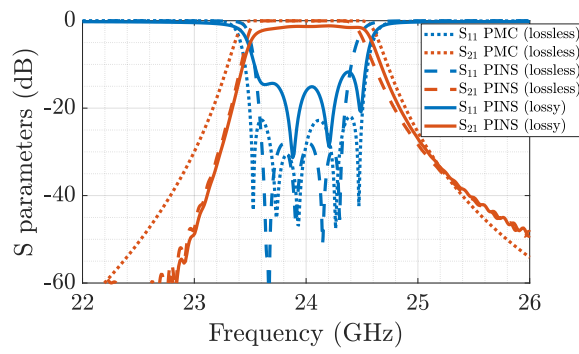

(**a**) Inverted microstrip gap waveguide technology and end-coupled lines discontinuity effect.
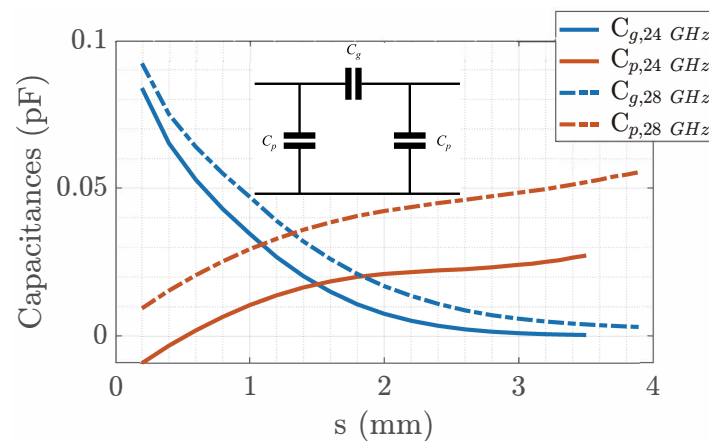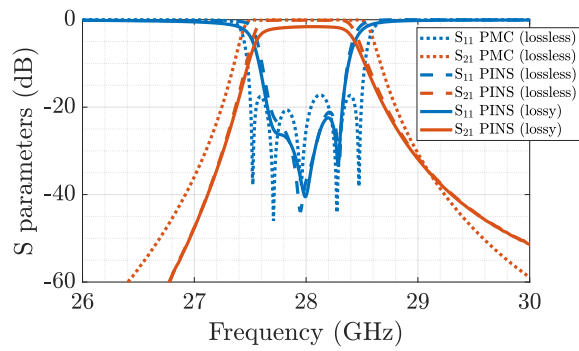

(**b**) Inset with discontinuity model with π-network capacitors and simulated values of the capacitances for different gap sizes.
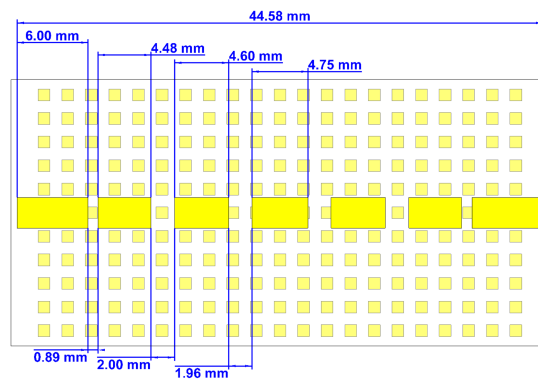
Figure 2. Line geometry and discontinuity model.
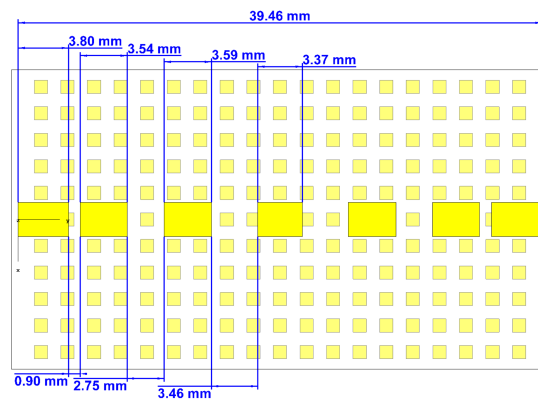
(**a**) 24 GHz inverted microstrip gap filter.

(**b**) 28 GHz inverted microstrip gap filter.

(**c**) Dimensions of the 24 GHz inverted microstrip filter with pins.


(**d**) Dimensions of the 28 GHz inverted microstrip filter with pins dimensions.

Figure 3. Filter comparison with PMC vs lossless PINS and vs lossy PINS.
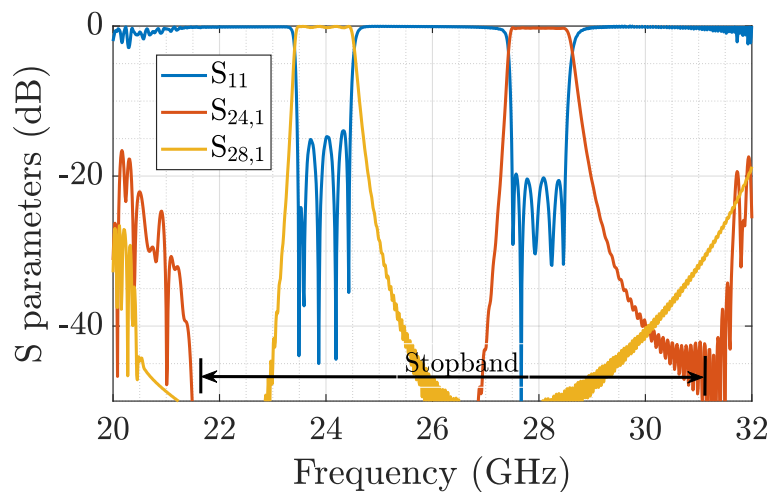
2.3. Diplexer Design

To design the diplexer, a power divider based on the rejection of the frequencies of the opposite arms with $\lambda/4$ transformers at the opposite frequency is implemented [42]. In this way, all the power is diverted to one filter or to the other, depending on the frequency.

Once the lengths of the divider arms were calculated as indicated before, using these as initial starting values, the filters were added for fine tuning with full wave simulations whose final design physical aspect is shown in Figure 4a. The simulated results for the lossless case implemented with pins is shown in Figure 4b where the good performance of the diplexer is observed. In the same figure, it is possible to clearly observe the limits of the stopband of the structure as an increase in the coupling.
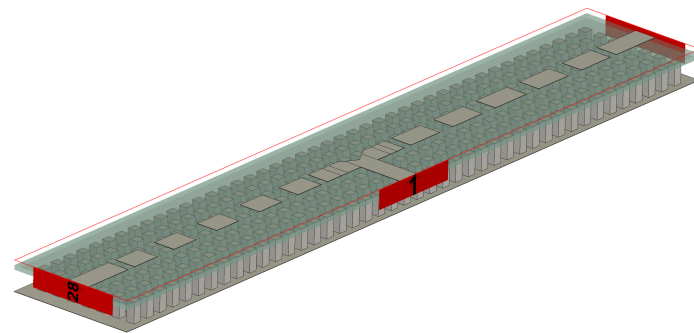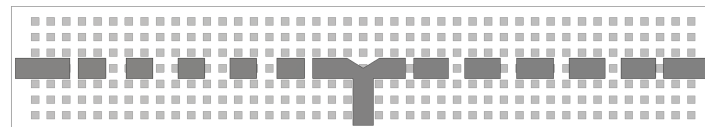
(**a**) Diplexer: 3D model with semi-transparent upper metal plate.

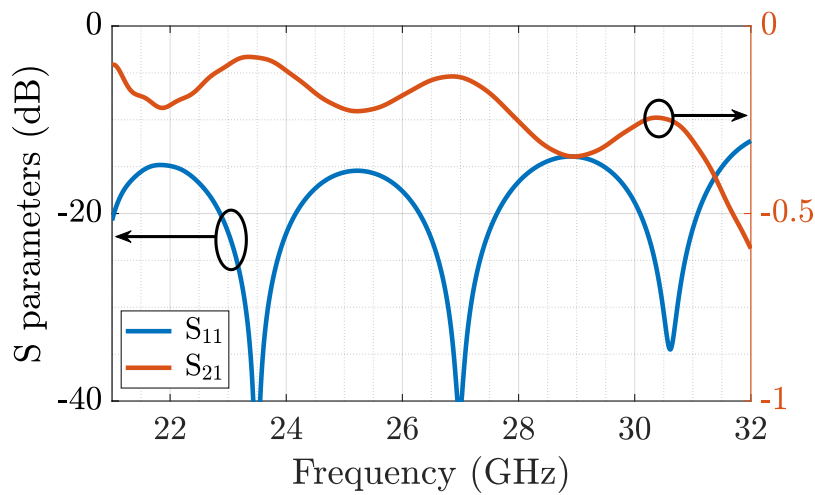(**b**) Simulated S-parameters of the diplexer using the bed of nails and lossless materials.

Figure 4. Diplexer design with lossless materials.

2.4. Inverted Microstrip Gap to Microstrip Transition Design

For the practical realization and measurement of this diplexer, a transition to conventional microstrip technology is necessary, where the EndLaunch connectors will be placed. To do this, we have followed the design guidelines found in [15] using the same substrate as for the diplexer. This results in a well-matched and low loss transition as can be seen in Figure 5b. In Figure 5a the geometry of the transition is shown.
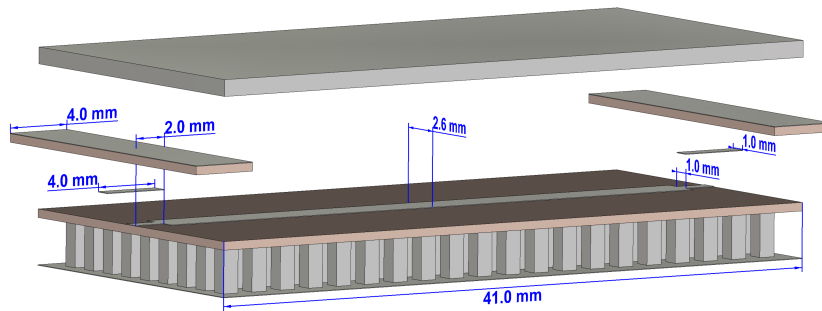
(**a**) Inverted Microstrip Gap Waveguide to Microstrip Transition Geometry.

(**b**) Simulated S-parameters of the inverted microstrip gap to microstrip transition.
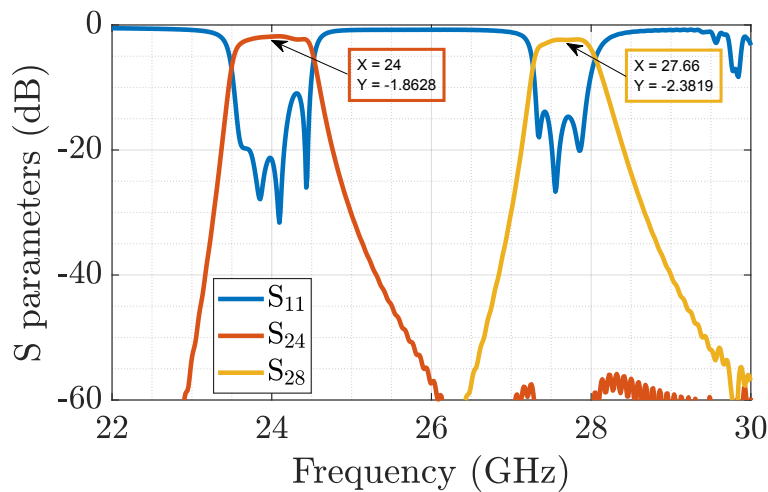
(**c**) Simulated S-parameters of the diplexer with the transitions.

Figure 5. Microstrip to Inverted Microstrip Gap Waveguide designed transition and final diplexer design with RO4003C$^{\text{TM}}$ substrate.

2.5. Losses Study

However, when simulating the diplexer including lossy materials and the inverted microstrip to microstrip transition, the losses are much higher than those predicted by the separate filters, as shown in Figure 5c. Still, the overall losses as a diplexer are much lower than for the examples made in standard microstrip technology in the Ka-band [35,43–46]. Nevertheless, a careful analysis of the

origin of the losses was made. In Figure 6 it is possible to observe that most of the losses come from the RO4003C^{TM} substrate. For this reason, we decided to do a re-design of the circuit using a new dielectric with lower losses, in particular, the RT5880^{TM} with ε_r = 2.2 and tanδ = 0.0009. Obviously, the design with a dielectric with lower losses will be more expensive.
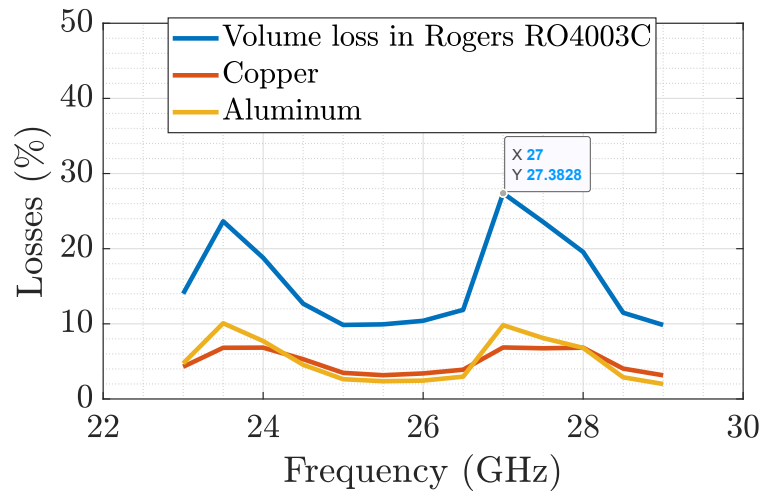

Figure 6. Material losses study as a function of the frequency.

### 2.6. Low Loss Rogers^{TM} 5880 Substrate Design

As mentioned, everything was redesigned using the new dielectric with lower losses, Rogers^{TM} 5880 (ε_r = 2.2 and tanδ = 0.0009 @10 GHz). First, the discontinuity model values were recalculated with the new substrate. After that, and following the same workflow, the filters were readjusted independently and, later, the diplexer as a whole was optimized.

The replacement of the RO4003C^{TM} substrate by the RT5880^{TM} in the unit cell, does not modify excessively the dispersion diagram and its stopband (seen in Figure 1). However, we decided to modify the height of the pins from 3.0 mm to 2.8 mm because it was found that the proximity of the stopband to the 28 GHz channel caused some problems in its performance in transmission. The change in the height moves up the upper limit of the stop band as observed in Figure 1 and it is summarized in Table 1.

Table 1. Dispersion diagram stopband limits.

Substrate	h pin	Finf (GHz)	Fsup (GHz)
RO4003C	3 mm	18.10	29.66
RT5880	3 mm	19.93	31.70
RT5880	2.8 mm	21.07	33.12

Figure 7 shows how the height of the pins affects the performance of the designed diplexer. In Figure 8 the final result for the diplexer with the chosen 2.8 mm pin height is shown. Finally, in Figure 9 the normalized absolute value of the E-field in the cross section at half the height of the gap of the RT5880^{TM} substrate is represented to show the qualitative behavior of the diplexer.
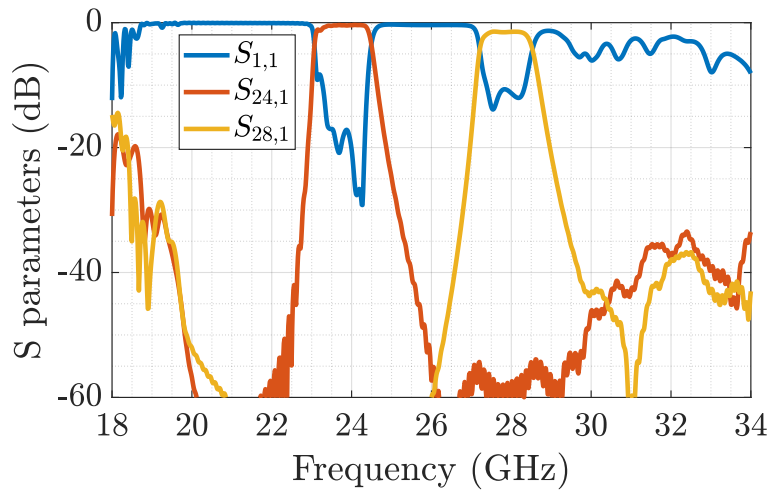
(**a**) Pin Height 3.0 mm.
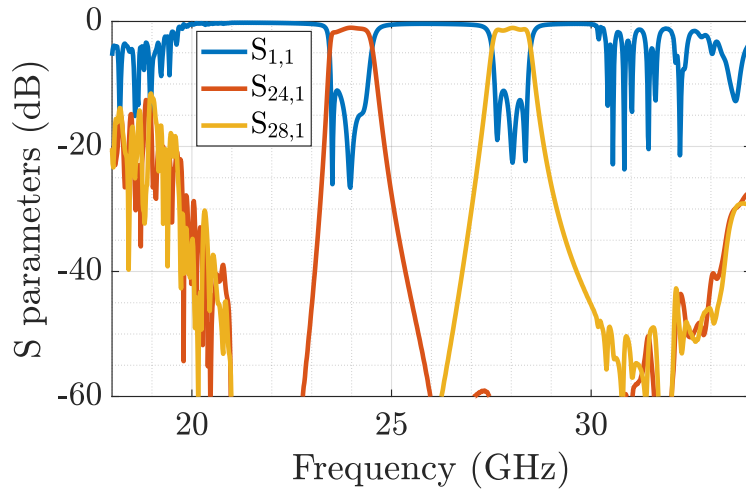
(**b**) Pin Height 2.8 mm.
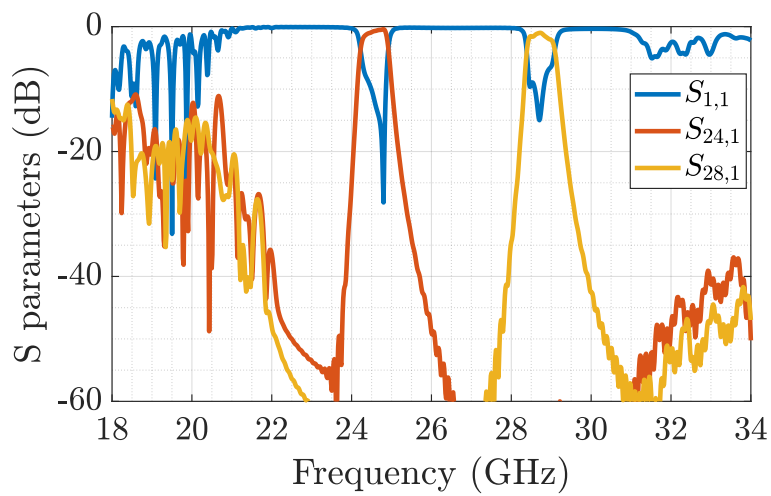
(**c**) Pin Height 2.6 mm.

Figure 7. S-parameters for RT5880^{TM} substrate diplexer vs stopband due to pin height.

(**a**) General view.

(**b**) Zoom

Figure 8. Diplexer S-parameters with lossy RT5880$^{\text{TM}}$ substrate and metals (pin height = 2.8 mm).
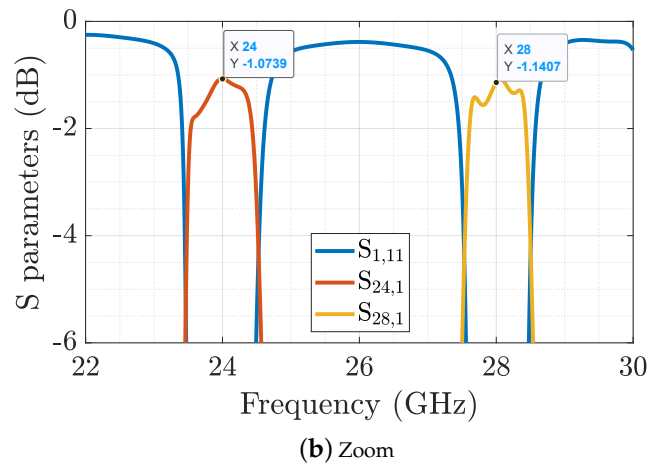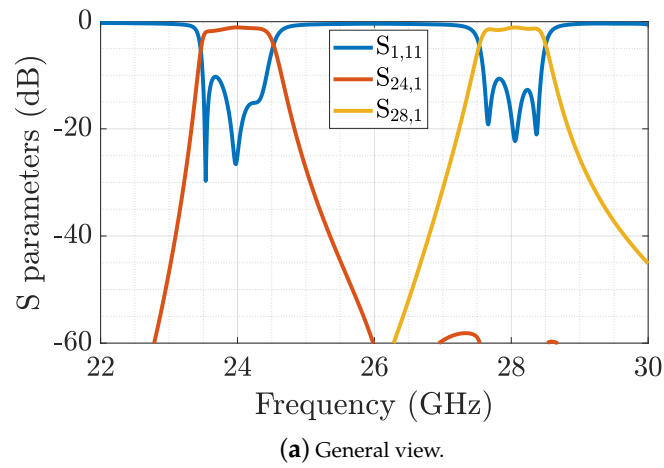

(**a**) E field @28 GHz channel visualization.

(**b**) E field @24 GHz channel visualization.

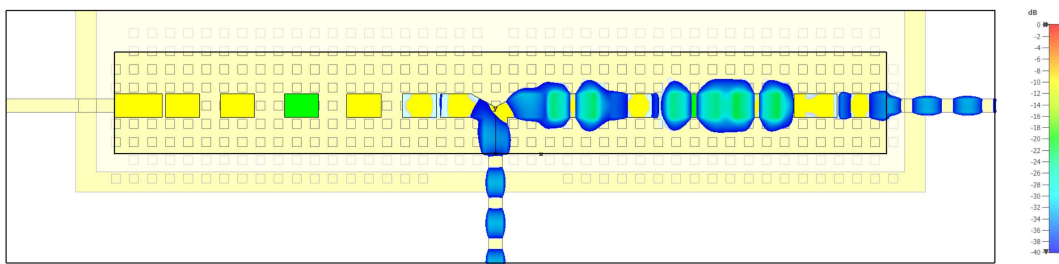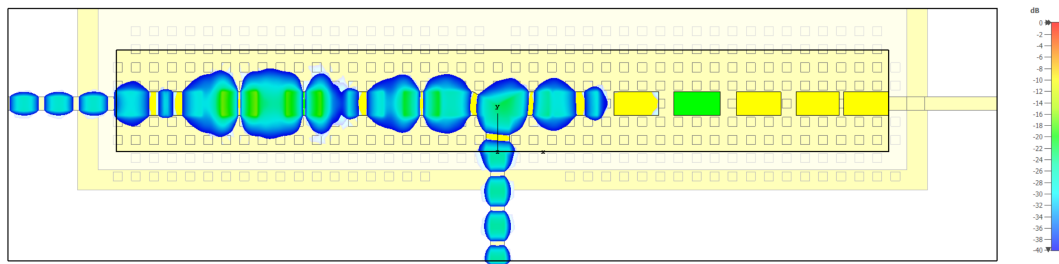**Figure 9.** Normalized to maximum absolute dB value E field cross section at half height gap of RT5880$^{\text{TM}}$ substrate diplexer.

3. Mechanical Design, Fabrication and Measurement

The diplexer geometry is shown in Figure 10a, and in Figure 10b–d the detailed dimensions of the prototype are described. Note that the circuit is not symmetrical, as the 28 GHz arm is shorter than the 24 GHz one. Finally, in Figure 11 the manufactured diplexer is shown both assembled and with all the pieces.

After TRL calibration to remove the effect of the End-Launch connectors, in Figure 12 the measured S-parameters are shown together with the corresponding simulations. Insertion losses at 24 GHz and 28 GHz band are 1.4 dB and 2 dB, respectively, both higher than in simulations, but still very low. It must be taken into account that the transition losses are included in these total measured insertion losses. We can see that the filters have shifted a bit in frequency towards the high band, probably due to uncertainties in the value of the dielectric constant.
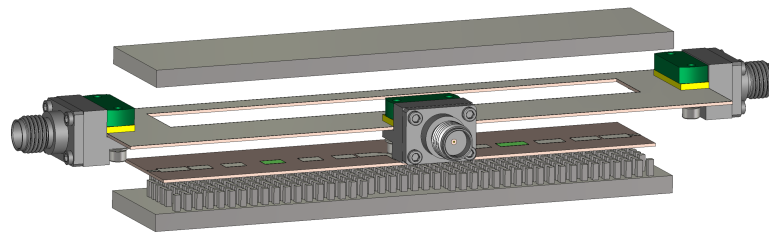
(**a**) 3D Inverted Microstrip Gap Diplexer geometry.
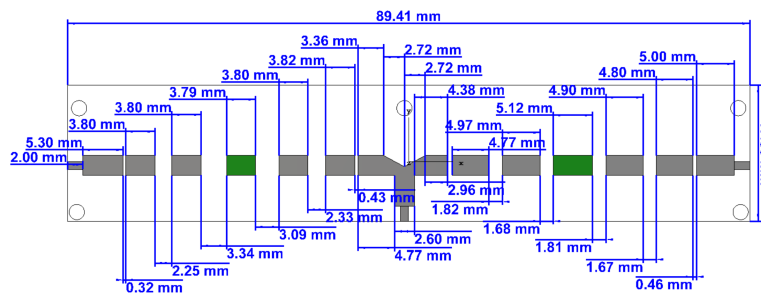
(**b**) Diplexer dimensions.
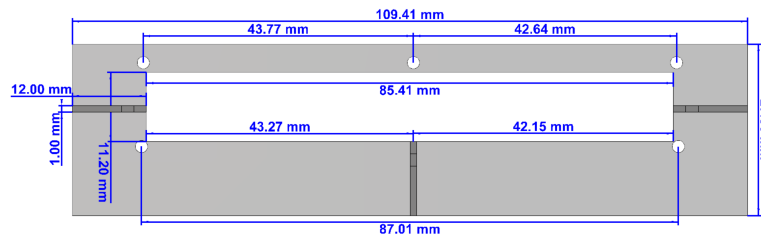
(**c**) Transition dimensions.

(**d**) Bed of nails dimensions.

Figure 10. Inverted Microstrip Gap Diplexer geometry and dimensions.

(**a**) Parts breakdown of diplexer.
(**b**) Top of assembled diplexer with transition and connectors.

Figure 11. Diplexer mounting and assembly.
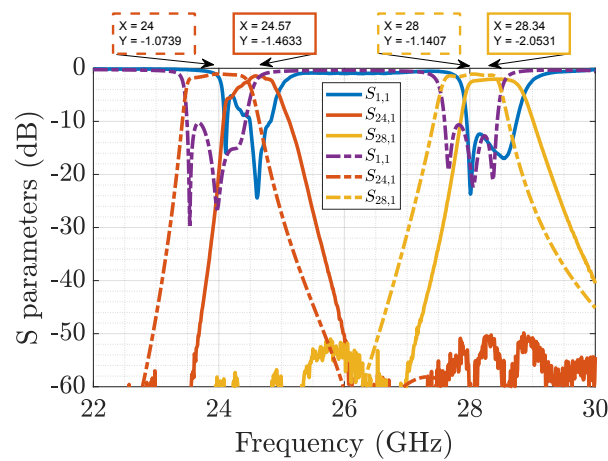
Figure 12. Measured vs simulated S-Parameters of Ka-band diplexer with RT5880$^{\text{TM}}$ in inverted microstrip gap waveguide technology (pin height = 2.8 mm).

Comparison with Other Measured Diplexers

If we put the figures of merit of the designed diplexer in inverted microstrip gap waveguide technology in perspective with other designs (shown in Table 2), we see that the performance is similar or even better with respect to insertion los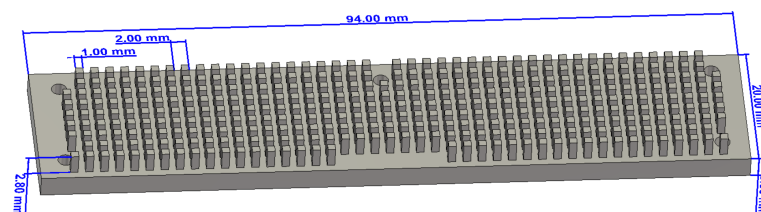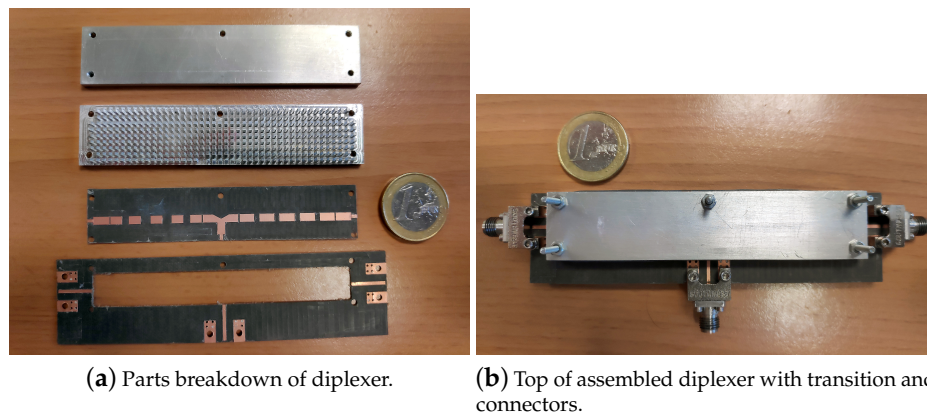ses, but using more affordable technology. In our estimation of the costs in the table, we consider very low cost technology only the standard printed technology. Classical waveguide technology and groove and ridge versions of gap waveguide technology are considered high cost. More sophisticated technologies are classified as very high cost. The proposed technology will have a similar cost as SIW technology and they are classified as low cost ones.

Table 2. Comparison with other mm-Wave measured diplexers.

	f_0 (GHz)	IL (dB)	Isol (dB)	BW (%)	Cost	Type
[47]	35	0.35	NA	1.7	High	Waveguide
[48]	66	1.5	50	59	Very High	Waveguide + SSL
[49]	20	4	50	2.4	Very High	Cryo-Microstrip
[50]	30	1.4	35	5	Very High	Membrane coupled microstrip
[51]	60	2.5	25	8.8	Very High	LCP (Liquid Crystal Polymer)
[52]	60	0.9	60	1.7	High	Groove Gap WG
[53]	35	3.5	30	3.7	Very Low	Classic Microstrip
[54]	60	6	30	6.25	Low	SIW
Our	28	2	60	3.5	Low	Inverted Microstrip Gap WG

4. Conclusions

A diplexer designed in inverted microstrip gap waveguide technology for the low part of the millimeter frequency range has been presented. The diplexer can be applied in the future expansion of the spectrum of the new 5G and beyond mobile communications standards. The designed diplexer is based on a classical design, other more advanced designs as the ones proposed for low frequencies in [55,56] could be also translated in the proposed IMGW technology. The diplexer works for two channels at 24 GHz and 28 GHz, with a bandwidth of approximately 1 GHz and the lowest possible ripple in the passband. Filters were implemented using the end-coupled band pass topology. The initial design was made using Rogers RO4003C^{TM} substrate, and although acceptable insertion losses were observed a re-design using RT5880^{TM} substrate was made to further decrease them. The measurements show good agreement with simulations, except for a slight frequency shift easily explainable by the discrepancy between the permittivity of the simulated material and the one of the actual substrate, as it was tested with simulations. The insertion losses are of 1.5 dB and 2 dB for 24 GHz and 28 GHz respectively, and a 60 dB isolation between channels is achieved. Comparing to other mm-Wave diplexers, this work offers a cost efficient and low losses alternative, especially when it is compared to the other versions of gap waveguide technology, i.e., groove and ridge. Furthermore, this technology allows easy integration of active elements and aperture antennas.

Author Contributions: Conceptualization, L.F.H. and E.R.-I.; Investigation, C.S.-C.; Methodology, C.S.-C. and E.R.-I.; Supervision, L.F.H. and E.R.-I.; Validation, L.F.H.; Writing—original draft, C.S.-C.; Writing—review and editing, L.F.H. and E.R.-I. All authors have read and agreed to the published version of the manuscript.

Abbreviations

The following abbreviations are used in this manuscript:

AMC   Artificial Magnetic Conductor
CST   Computer Simulation Studio
PMC   Perfect Magnetic Conductor
TEM   Transverse Electromagnetic Mode

References

1. Kildal, P.; Alfonso, E.; Valero-Nogueira, A.; Rajo-Iglesias, E. Local Metamaterial-Based Waveguides in Gaps Between Parallel Metal Plates. *IEEE Antennas Wirel. Propag. Lett.* **2009**, *8*, 84–87. [CrossRef]
2. Kildal, P.; Zaman, A.U.; Rajo-Iglesias, E.; Alfonso, E.; Valero-Nogueira, A. Design and experimental verification of ridge gap waveguide in bed of nails for parallel-plate mode suppression. *IET Microw. Antennas Propag.* **2011**, *5*, 262–270. [CrossRef]
3. Rajo-Iglesias, E.; Zaman, A.U.; Kildal, P. Parallel Plate Cavity Mode Suppression in Microstrip Circuit Packages Using a Lid of Nails. *IEEE Microw. Wirel. Components Lett.* **2010**, *20*, 31–33. [CrossRef]
4. Rajo-Iglesias, E.; Kildal, P. Numerical studies of bandwidth of parallel-plate cut-off realised by a bed of nails, corrugations and mushroom-type electromagnetic bandgap for use in gap waveguides. *IET Microw. Antennas Propag.* **2011**, *5*, 282–289. [CrossRef]
5. Berenguer, A.; Baquero-Escudero, M.; Sanchez-Escuderos, D.; Vico, F. Suspended-strip gap waveguide coupled-line properties for Ka-band component design. In Proceedings of the 2015 9th European Conference on Antennas and Propagation (EuCAP), Lisbon, Portugal, 13–17 April 2015; pp. 1–5.
6. Pucci, E.; Zaman, A.U.; Rajo-Iglesias, E.; Kildal, P. New low loss inverted microstrip line using gap waveguide technology for slot antenna applications. In Proceedings of the 5th European Conference on Antennas and Propagation (EUCAP), Rome, Italy, 11–15 April 2011; pp. 979–982.
7. Pucci, E.; Rajo-Iglesias, E.; Kildal, P. New Microstrip Gap Waveguide on Mushroom-Type EBG for Packaging of Microwave Components. *IEEE Microw. Wirel. Components Lett.* **2012**, *22*, 129–131. [CrossRef]

8. Liu, J.; Yang, J.; Zaman, A.U. Study of Dielectric Loss and Conductor Loss among Microstrip, covered Microstrip and inverted Microstrip Gap Waveguide utilizing variational Method in Millimeter Waves. In Proceedings of the 2018 International Symposium on Antennas and Propagation (ISAP), Busan, Korea, 23–26 October 2018; pp. 1–2.

9. Rajo-Iglesias, E.; Ferrando-Rocher, M.; Zaman, A.U. Gap Waveguide Technology for Millimeter-Wave Antenna Systems. *IEEE Commun. Mag.* **2018**, *56*, 14–20. [CrossRef]

10. Liu, J.; Yang, J.; Zaman, A.U. Analytical Solutions to Characteristic Impedance and Losses of Inverted Microstrip Gap Waveguide Based on Variational Method. *IEEE Trans. Antennas Propag.* **2018**, *66*, 7049–7057. [CrossRef]

11. Pizarro, F.; Sanchez-Cabello, C.; Vazquez-Roy, J.L.; Rajo-Iglesias, E. Considerations of impedance sensitivity and losses in designing inverted microstrip gap waveguides. *AEU Int. J. Electron. Commun.* **2020**, *124*, 153353. doi:10.1016/j.aeue.2020.153353. [CrossRef]

12. Brazález, A.A.; Iglesias, E.R.; Kildal, P. Investigation of transitions for use in inverted microstrip gap waveguide antenna arrays. In Proceedings of the The 8th European Conference on Antennas and Propagation (EuCAP 2014), The Hague, The Netherlands, 6–11 April 2014; pp. 995–999. [CrossRef]

13. Brazález, A.A.; Rajo-Iglesias, E.; Vázquez-Roy, J.L.; Vosoogh, A.; Kildal, P. Design and Validation of Microstrip Gap Waveguides and Their Transitions to Rectangular Waveguide, for Millimeter-Wave Applications. *IEEE Trans. Microw. Theory Tech.* **2015**, *63*, 4035–4050. [CrossRef]

14. Brazález, A.A.; Rajo-Iglesias, E.; Kildal, P. Design of millimeter-wave wideband gap waveguide transitions considering integration into the antenna system. In Proceedings of the 2015 9th European Conference on Antennas and Propagation (EuCAP), Lisbon, Portugal, 13–17 April 2015; pp. 1–5.

15. Rajo-Iglesias, E.; Brazález, A.A. 5G antenna in inverted microstrip gap waveguide technology including a transition to microstrip. In Proceedings of the 2016 International Symposium on Antennas and Propagation (ISAP), Okinawa, Japan, 24–28 October 2016; pp. 1042–1043.

16. Liu, J.; Zaman, A.U.; Kildal, P. Design of transition from WR-15 to inverted microstrip gap waveguide. In Proceedings of the 2016 Global Symposium on Millimeter Waves (GSMM) ESA Workshop on Millimetre-Wave Technology and Applications, Espoo, Finland, 6–8 June 2016; pp. 1–4. [CrossRef]

17. Jinlin, L.; Zaman, A.U.; Kildal, P. Optimizing the numerical port for inverted microstrip gap waveguide in full-wave simulators. In Proceedings of the 2016 10th European Conference on Antennas and Propagation (EuCAP), Davos, Switzerland, 10–15 April 2016; pp. 1–5. [CrossRef]

18. Pucci, E.; Kildal, P.; Rajo-Iglesias, E.; Vazquez-Roy, J. Design of a four-element horn antenna array fed by inverted microstrip gap waveguide. In Proceedings of the 2013 IEEE Antennas and Propagation Society International Symposium (APSURSI), Orlando, FL, USA, 7–13 July 2013; pp. 1226–1227. [CrossRef]

19. Sanchez-Cabello, C.; Rajo-Iglesias, E. Low cost self-diplexed antenna in inverted microstrip gap waveguide technology. In Proceedings of the 2014 International Symposium on Antennas and Propagation Conference Proceedings, Kaohsiung, Taiwan, 2–5 December 2014; pp. 169–170. [CrossRef]

20. Pucci, E.; Rajo-Iglesias, E.; Vázquez-Roy, J.; Kildal, P. Planar Dual-Mode Horn Array With Corporate-Feed Network in Inverted Microstrip Gap Waveguide. *IEEE Trans. Antennas Propag.* **2014**, *62*, 3534–3542. [CrossRef]

21. Razavi, S.A.; Kildal, P. An air-filled cavity-backed 2 × 2 slot sub-array fed by inverted microstrip gap waveguide. In Proceedings of the 2015 9th European Conference on Antennas and Propagation (EuCAP), Lisbon, Portugal, 13–17 April 2015; pp. 1–4.

22. Liu, J.; Vosoogh, A.; Zaman, A.U.; Kildal, P. Design of a cavity-backed slot array unit cell on inverted microstrip gap waveguide. In Proceedings of the 2015 International Symposium on Antennas and Propagation (ISAP), Hobart, TAS, Australia, 9–12 November 2015; pp. 1–4.

23. Sanchez-Cabello, C.; Rajo-Iglesias, E. Optimized self-diplexed antenna in gap waveguide technology. In Proceedings of the 2015 IEEE International Symposium on Antennas and Propagation USNC/URSI National Radio Science Meeting, Vancouver, BC, Canada, 19–24 July 2015; pp. 460–461. [CrossRef]

24. Liu, J.; Vosoogh, A.; Zaman, A.U.; Kildal, P. Design of 8 x 8 slot array antenna based on inverted microstrip gap waveguide. In Proceedings of the 2016 International Symposium on Antennas and Propagation (ISAP), Okinawa, Japan, 24–28 October 2016; pp. 760–761.

25. Zaman, A.U.; Kildal, P. Different gap waveguide slot array configurations for mmwave fixed beam antenna application. In Proceedings of the 2016 10th European Conference on Antennas and Propagation (EuCAP), Davos, Switzerland, 10–15 April 2016; pp. 1–4. [CrossRef]

26. Liu, J.; Vosoogh, A.; Zaman, A.U.; Yang, J. Design and Fabrication of a High-Gain 60-GHz Cavity-Backed Slot Antenna Array Fed by Inverted Microstrip Gap Waveguide. *IEEE Trans. Antennas Propag.* **2017**, *65*, 2117–2122. [CrossRef]

27. Liu, J.; Vosoogh, A.; Zaman, A.U.; Yang, J. Slot antenna array unit cell directly fed by inverted microstrip gap waveguide. In Proceedings of the 2017 International Symposium on Antennas and Propagation (ISAP), Phuket, Thailand, 30 October–2 November 2017; pp. 1–2. [CrossRef]

28. Cao, J.; Wang, H.; Mou, S.; Liu, S. W-band High-Performance Cavity-backed Slot Antenna Array with Inverted Microstrip Gap Waveguide. In Proceedings of the 2018 IEEE International Symposium on Antennas and Propagation USNC/URSI National Radio Science Meeting, Boston, MA, USA, 8–13 July 2018; pp. 1039–1040. [CrossRef]

29. Liu, J.; Zaman, A.U.; Yang, J. A Low Sidelobe Double-Layer Corporate-Feed Array Antenna by Inverted Microstrip Gap Waveguide at 28 GHz. In Proceedings of the 2019 International Symposium on Antennas and Propagation (ISAP), Xi'an, China, 27–30 October 2019; pp. 1–4.

30. Zhang, T.; Chen, L.; Moghaddam, S.M.; Uz Zaman, A.; Yang, J. Ultra-wideband Circularly Polarized Planar Array Antenna Using Single-Arm-Spiral Elements and Dielectric-based IMGW. In Proceedings of the 2019 International Symposium on Antennas and Propagation (ISAP), Xi'an, China, 27–30 October 2019; pp. 1–3.

31. Zhang, T.; Chen, L.; Moghaddam, S.M.; Uz Zaman, A.; Yang, J. Wideband Dual-polarized Array Antenna on Dielectric-based Inverted Microstrip Gap Waveguide. In Proceedings of the 2019 13th European Conference on Antennas and Propagation (EuCAP), Krakow, Poland, 31 March–5 April 2019; pp. 1–3.

32. Zhang, T.; Chen, L.; Moghaddam, S.M.; Zaman, A.U.; Yang, J. Ultra-wideband linearly polarised planar bowtie array antenna with feeding network using dielectric-based inverted microstrip gap waveguide. *IET Microw. Antennas Propag.* **2020**, *14*, 485–490. [CrossRef]

33. Algaba-Brazalez, A.; Rajo-Iglesias, E. Design of a Butler matrix at 60 GHz in inverted microstrip gap waveguide technology. In Proceedings of the 2015 IEEE International Symposium on Antennas and Propagation USNC/URSI National Radio Science Meeting, Vancouver, BC, Canada, 19–24 July 2015; pp. 2125–2126. [CrossRef]

34. Pizarro, F.; Ramírez-Gil, D.; Algaba-Brazález, A.; Herrán-Ontanón, L.F.; Rajo-Iglesias, E. Comparison study of 4 × 4 Butler matrices in microstrip technologies for Ka-band. *AEU Int. J. Electron. Commun.* **2020**, *122*, 153248. [CrossRef]

35. Sorkherizi, M.S.; Kishk, A.A. Lowloss planar bandpass filters for millimeter-wave application. In Proceedings of the 2015 IEEE MTT-S International Microwave Symposium, Phoenix, AZ, USA, 17–22 May 2015; pp. 1–4. [CrossRef]

36. Vosoogh, A.; Brazález, A.A.; Kildal, P. A V-Band Inverted Microstrip Gap Waveguide End-Coupled Bandpass Filter. *IEEE Microw. Wirel. Components Lett.* **2016**, *26*, 261–263. [CrossRef]

37. Sharifi Sorkherizi, M.; Kishk, A.A. Fully Printed Gap Waveguide With Facilitated Design Properties. *IEEE Microw. Wirel. Components Lett.* **2016**, *26*, 657–659. [CrossRef]

38. Inclan-Sanchez, L.; Sanchez-Cabello, C.; Vazquez-Roy, J.L.; Rajo-Iglesias, E. New EBG-filter design in inverted microstrip gap waveguide technology. In Proceedings of the 2017 IEEE International Symposium on Antennas and Propagation USNC/URSI National Radio Science Meeting, San Diego, CA, USA, 9–14 July 2017; pp. 1663–1664. [CrossRef]

39. Deng, J.; Li, M.; Sun, D.; Guo, L.; Ma, X. Compact Dual-Band Inverted-Microstrip Ridge Gap Waveguide Bandpass Filter. *IEEE Trans. Microw. Theory Tech.* **2020**, *68*, 2625–2632. [CrossRef]

40. Vosoogh, A.; Sorkherizi, M.S.; Zaman, A.U.; Yang, J.; Kishk, A.A. An Integrated Ka-Band Diplexer-Antenna Array Module Based on Gap Waveguide Technology With Simple Mechanical Assembly and No Electrical Contact Requirements. *IEEE Trans. Microw. Theory Tech.* **2018**, *66*, 962–972. [CrossRef]

41. Lowpass and Bandpass Filters. In *Microstrip Filters for RF/Microwave Applications*; John Wiley & Sons, Inc., : Hoboken, NJ, USA, 2011; pp. 112–161. [CrossRef]

42. Jung, D.; Chang, K. Microstrip diplexer design for X-band RF/microwave front-end applications. In Proceedings of the 2011 IEEE International Symposium on Antennas and Propagation (APSURSI), Spokane, WA, USA, 3–8 July 2011; pp. 5–7. [CrossRef]

43. Zhao, W.; Zhang, Y.; Guo, Y. A novel Ka-band bandpass filter using microstrip closed loop resonators. In Proceedings of the 2009 Asia Pacific Microwave Conference, Singapore, 7–10 December 2009; pp. 1443–1445. [CrossRef]

44. Zhang, Q.; Dong, Y.; Cao, J. Dual-mode bandpass filter using microstrip SIR at Ka band. In Proceedings of the 2009 Asia Pacific Microwave Conference, Singapore, 7–10 December 2009; pp. 1401–1404. [CrossRef]

45. Mbeutcha, M.; Johansen, T.K.; Dong, Y.; Cimoli, B.; Krozer, V. Replicability of a Millimeter-Wave Microstrip Bandpass Filter using Parallel Coupled Lines. In Proceedings of the 2018 IEEE MTT-S Latin America Microwave Conference (LAMC 2018), Arequipa, Peru, 12–14 December 2018; pp. 1–3. [CrossRef]

46. Keskin, A.K.; Dagcan Senturk, M.; Demirel, S.; Kizilay, A.; Turk, A.S. Front-end design for Ka band mm-Wave radar. In Proceedings of the 2016 17th International Radar Symposium (IRS), Krakow, Poland, 10–12 May 2016; pp. 1–4. [CrossRef]

47. Liu, Z.; Zhang, R.; Hua, T. Design of Ka-band practical waveguide duplexer. In Proceedings of the 2016 CIE International Conference on Radar (RADAR), Guangzhou, China, 10–13 October 2016; pp. 1–3. [CrossRef]

48. Ashiq, I.; Khanna, A. A novel ultra-broadband DC-36-to-66-GHz hybrid diplexer using waveguide and SSL technology. In Proceedings of the 2014 44th European Microwave Conference, Rome, Italy, 6–9 October 2014; pp. 1111–1114, [CrossRef]

49. Setoodeh, S.; Mansour, R.R.; Gupta, D. Multi-layer low temperature superconducting K-band filter and diplexer design. In Proceedings of the 2013 IEEE MTT-S International Microwave Symposium Digest (MTT), Seattle, WA, USA, 2–7 June 2013; pp. 1–4. [CrossRef]

50. Brown, A.R.; Rebeiz, G.M. A high-performance integrated K-band diplexer. *IEEE Trans. Microw. Theory Tech.* **1999**, *47*, 1477–1481. [CrossRef]

51. Bairavasubramanian, R.; Pinel, S.; Laskar, J.; Papapolymerou, J. Compact 60-GHz bandpass filters and duplexers on liquid crystal polymer technology. *IEEE Microw. Wirel. Components Lett.* **2006**, *16*, 237–239. [CrossRef]

52. Rezaee, M.; Zaman, A.U. Realisation of carved and iris groove gap waveguide filter and E-plane diplexer for V-band radio link application. *IET Microwaves Antennas Propag.* **2017**, *11*, 2109–2115. [CrossRef]

53. Hong, S.; Chang, K. Stub-tuned microstrip bandpass filters for millimeter-wave diplexer design. *IEEE Microw. Wirel. Components Lett.* **2005**, *15*, 582–584. [CrossRef]

54. Wang, D.; Chin, K.; Che, W.; Chang, C.; Wu, Y. 60 GHz duplexer design using dual-mode SIW filters with single-sided transmission zeros. *Electron. Lett.* **2014**, *50*, 1529–1531. [CrossRef]

55. Zurek, P.; Cappello, T.; Popovic, Z. Broadband Diplexed Power Amplifier. *IEEE Microw. Wirel. Components Lett.* **2020**, *30*, 1073–1076. [CrossRef]

56. Rezaei, A.; Noori, L. Miniaturized microstrip diplexer with high performance using a novel structure for wireless L-band applications. *Wirel. Netw.* **2020**, *26*, 1795–1802. [CrossRef]